



Article

Three-Dimensional Printed Porous Titanium Screw with Bioactive Surface Modification for Bone–Tendon Healing: A Rabbit Animal Model

Yu-Min Huang ^{1,2,3,†} , Chih-Chieh Huang ^{4,†}, Pei-I Tsai ⁵ , Kuo-Yi Yang ⁵, Shin-I Huang ⁵, Hsin-Hsin Shen ⁵, Hong-Jen Lai ⁶, Shu-Wei Huang ¹, San-Yuan Chen ⁴, Feng-Huei Lin ^{1,7} and Chih-Yu Chen ^{2,3,*}

¹ Department of Biomedical Engineering, National Taiwan University, Taipei 106, Taiwan; yellowcorn0326@yahoo.com.hk (Y.-M.H.); judyya1022@gmail.com (S.-W.H.); double@ntu.edu.tw (F.-H.L.)

² Department of Orthopedics, Shuang Ho Hospital, Taipei Medical University, Taipei 100, Taiwan

³ Department of Orthopedics, School of Medicine, College of Medicine, Taipei Medical University, Taipei 100, Taiwan

⁴ Department of Materials Science and Engineering, National Chiao-Tung University, Hsinchu 300, Taiwan; Sigher@itri.org.tw (C.-C.H.); sanyuanchen@mail.nctu.edu.tw (S.-Y.C.)

⁵ Biomedical Technology and Device Research Laboratories, Industrial Technology Research Institute, Hsinchu 310, Taiwan; peiyi@itri.org.tw (P.-I.T.); yangkuoyi@itri.org.tw (K.-Y.Y.); SophiaShinI@itri.org.tw (S.-I.H.); shenhsin@itri.org.tw (H.-H.S.)

⁶ Material and Chemical Research Laboratories, Industrial Technology Research Institute, Hsinchu 310, Taiwan; hjlai@itri.org.tw

⁷ Institute of Biomedical Engineering and Nanomedicine, National Health Research Institutes, Miaoli County 360, Taiwan

* Correspondence: aleckc2424@gmail.com; Tel.: +886-970-747767

† Contributed equally.

Received: 23 April 2020; Accepted: 19 May 2020; Published: 21 May 2020



Abstract: The interference screw fixation method is used to secure a graft in the tibial tunnel during anterior cruciate ligament reconstruction surgery. However, several complications have been reported, such as biodegradable screw breakage, inflammatory or foreign body reaction, tunnel enlargement, and delayed graft healing. Using additive manufacturing (AM) technology, we developed a titanium alloy (Ti₆Al₄V) interference screw with chemically calcium phosphate surface modification technology to improve bone integration in the tibial tunnel. After chemical and heat treatment, the titanium screw formed a dense apatite layer on the metal surface in simulated body fluid. Twenty-seven New Zealand white rabbits were randomly divided into control and additive manufactured (AMD) screw groups. The long digital extensor tendon was detached and translated into a tibial plateau tunnel (diameter: 2.0 mm) and transfixed with an interference screw while the paw was in dorsiflexion. Biomechanical analyses, histological analyses, and an imaging study were performed at 1, 3, and 6 months. The biomechanical test showed that the ultimate pull-out load failure was significantly higher in the AMD screw group in all tested periods. Micro-computed tomography analyses revealed early woven bone formation in the AMD screw group at 1 and 3 months. In conclusion, AMD screws with bioactive surface modification improved bone ingrowth and enhanced biomechanical performance in a rabbit model.

Keywords: bioactive ceramic coating; interference screw; additive manufacturing; titanium-alloy implant

1. Introduction

Anterior cruciate ligament (ACL) tears are a common sports injury, and ACL reconstruction (ACLR) is the most performed procedure to restore knee stability to enable a return to sports [1]. The success of ACLR depends on graft healing and the type of fixation. Tibial fixation is commonly considered weaker than femoral fixation because the bone mineral density of the proximal tibia is lower than that of the distal femur [2,3]. Furthermore, the force vector of ACL grafts is parallel to the tibial tunnel, which places maximal force on the tibial graft fixation [2]. There are two major categories of interference screws used for ACLR, namely permanent metal screws and bioabsorbable screws. Bioabsorbable screw materials include polyglycolic acid, poly-L-lactic acid, and poly-D,L-lactic acid. Clinical outcomes have been equivalent after the use of bioabsorbable screws and metal interference screws for tibial graft fixation [4]; however, higher rates of effusion, screw breakage, and incomplete tunnel healing have been reported for bioabsorbable screws compared with titanium alloy (Ti) interference screws [5]. The rate of clinical sequelae from bioabsorbable tibial interference screws was high, with symptoms in approximately 1 of 10 ACLRs in adolescents [6]. Therefore, in this rabbit study, we selected Depuy Synthes Ti cortical screws as the control groups for tibial intratunnel healing and compared them with experimental screws of the same diameter and similar morphology. We evaluated the effects of Ti interference screws on tibial bone–tendon graft incorporation.

Titanium is a widely used metallic biomaterial with excellent fatigue and corrosion resistance [7]. To enhance bone integration, the modification of surface properties is thought to be able to improve the interaction and healing of tissue materials. White et al. [8] reported that porous materials can induce osteointegration. Clemow et al. [9] demonstrated that different Ti pore sizes can alter the shear force and bone ingrowth. Porous Ti samples stimulated faster osteoblast cell differentiation and ingrowth because of cell morphology changes within the Ti pores [10]. To augment further cell adhesion and tissue ingrowth, research has been devoted to bioactive ceramics on Ti implants [11]. Bioactive ceramics have a surface similar to the structure of bone and the ability to enhance bone tissue formation [12]. Plasma-sprayed hydroxyapatite (HA) coated on Ti has been commonly used; however, the heating process during coating results in undesirable HA decomposition and altered biocompatibility [13]. Moreover, Yang et al. reported that the different thermal expansion coefficients of HA and Ti₆Al₄V result in high tensile stress and poor adhesion [14]. Furthermore, differences in HA thickness may cause fractures inside the HA coating layer or at the HA–Ti interface [15]. Coating Ti implants with bioactive calcium phosphate (CaP) ceramic provides an osteoconductive surface that stimulates bone ingrowth and minimizes prosthesis loosening [11,16]. Aniket et al. reported that bioactive ceramic coatings can induce osteoblast-like cell accumulation and decrease inflammatory bone cell responses [17]. Tadashi et al. reported a novel bioactive titanate layer using chemical and heat treatments [18]. When Ti alloy was soaked in CaCl₂ solution after NaOH treatment, the sodium hydrogen titanate formed by NaOH was transformed into calcium hydrogen titanate. After heat treatment and soaking in simulated body fluid (SBF), the apatite formed on the surface of Ti because positively charged calcium ions and negatively charged phosphate ions formed CaP. After a subsequent water treatment, the titanate formed bone-like apatite on the surface of the titanate in SBF.

Implant designs can be improved through additive manufacturing (AM) technology, which offers engineers new design freedom [19]. AM technology, otherwise known as three-dimensional (3D) printing, is a process through which a 3D object is created by successively layering materials, such as liquids, biodegradable polymers, or metals. AM technology has been used for a controlled drug delivery system [20], regenerative medicine [21], and joint replacement design [22]. AM technologies are superior to conventional fabrication techniques for producing porous structures for bone ingrowth [23–25]. Furthermore, AM technology provides greater customizability, speed, and accuracy through computer-aided design. In our previous study, we illustrated how a porous Ti interference screw produced using AM technology could improve tibial graft fixation and enhance the biomechanical performance of the bone–tendon–screw construct [26]. We proposed that by using surface modification

technology, we could develop a novel interference screw with appropriate structural porosity and surface reactivity, which would improve graft fixation and enhance biomechanical performance.

2. Results

2.1. Additive Manufactured Interference Screw with Bioactive Surface Modification

In Figure 1, scanning electron microscopy (SEM) images clearly show a feather-like apatite nanostructure coated onto the surface of the additive manufactured (AMD) screw after bioactive surface modification. The apatite nanostructure had a diameter of approximately 50–100 nm, the thickness of the coating layer was approximately 1 μm , and the average pore size on the AMD screw was from 200 to 400 μm .

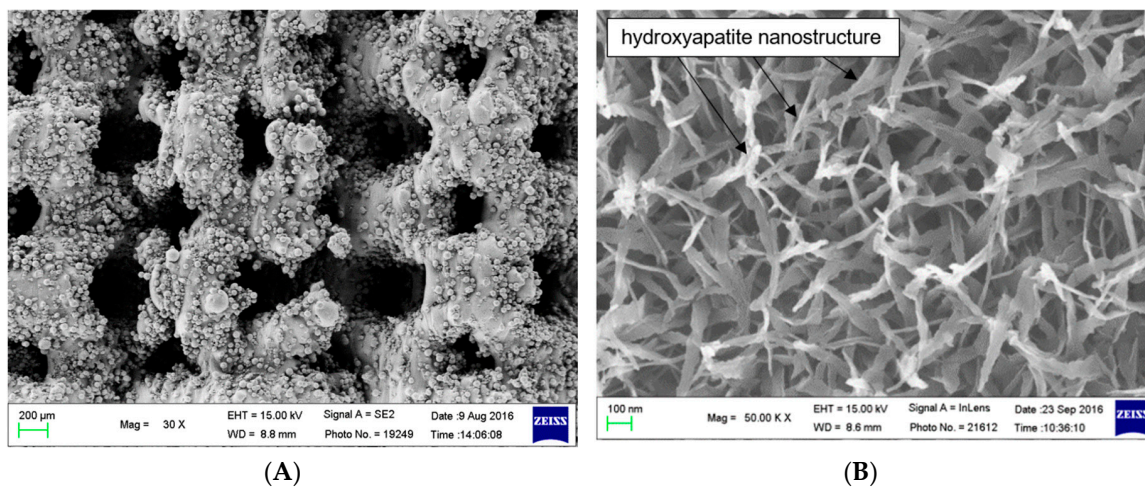


Figure 1. (A) Outer surface of the additive manufactured screw, low magnification. Scanning electron microscopy images of the surface of the additive manufactured screw, (B) Bioactive surface coating, high magnification. The SEM images reveal a diffuse feather-like apatite nanostructure coating on the Ti metal, which had been soaked in SBF for 3 days after NaOH and heat treatments.

In Figure 2, transmission electron micrograph (TEM) images illustrate the apatite formation on the AMD screw after surface modification. Bone-like apatite is formed on the surface of Titanium metal in SBF. The apatite formation on the surface layer is needle-like form, and has a composition with Ca/P ratio = 1.6 from the transmission electron micrograph and energy dispersive X-ray spectroscopy (EDX) (Figure 2C).

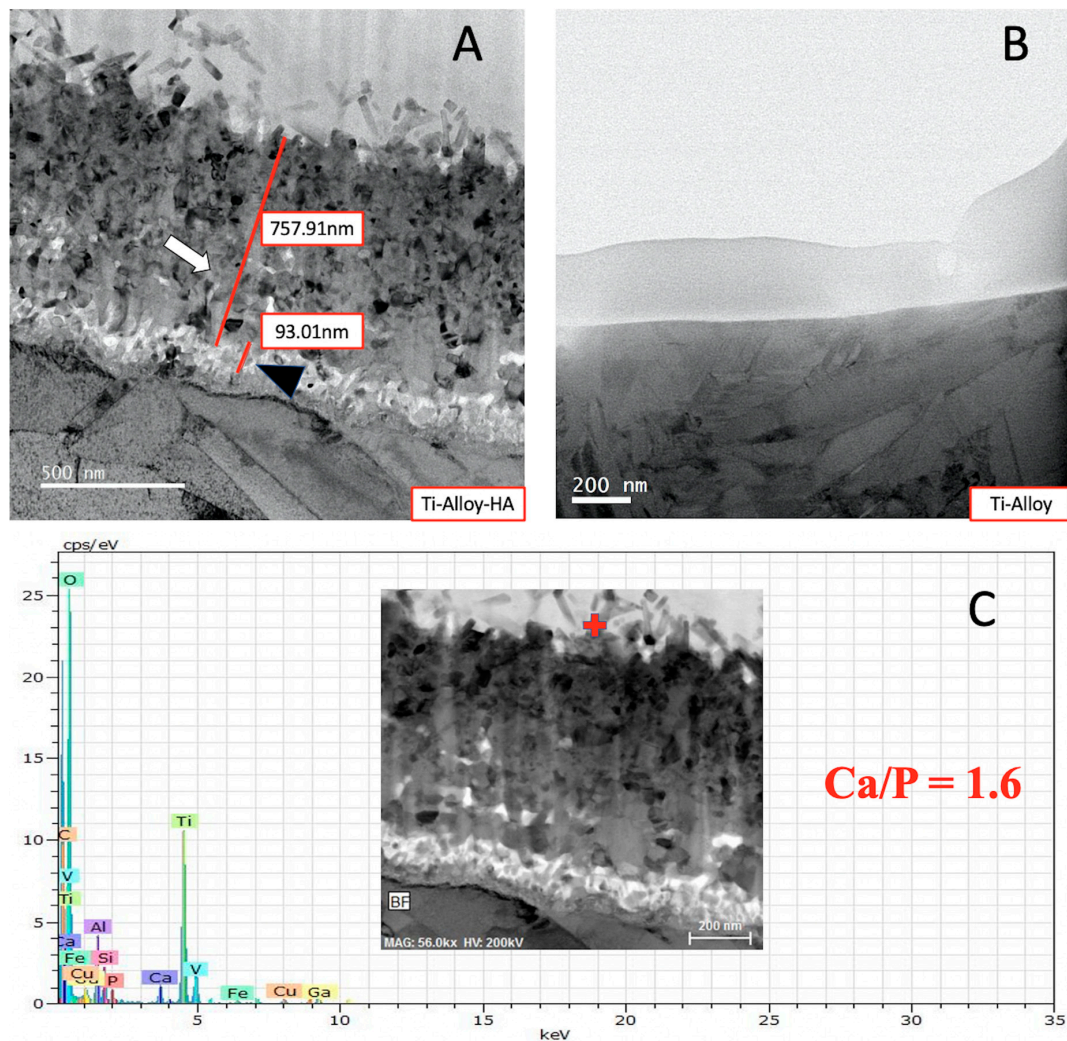


Figure 2. TEM photographs and EDX examination. (A) Ti-alloy with surface modification, formation of apatite can be seen on the Ti-alloy surface (white arrow), black arrowhead denotes anatase and rutile on the Ti-alloy surface. (B) Ti-alloy only. (C) EDX on the apatite of the Ti-alloy with surface modification. Red cross marks the area of electron diffraction and EDX analysis.

2.2. Biomechanical Analysis

In the biomechanical test, the ultimate load-to-failure in the AMD screw was consistently significantly higher than that in the control group at 1, 3, and 6 months (Figure 3). All specimens failed at the bone–tendon–screw junction in the tibial tunnel. The mean maximal load at failure was 43.3 ± 2.7 N in the control group compared with 56.6 ± 4.7 N in the AMD group in 6-month specimens ($p = 0.0001$). In both groups, the maximal failure load increased progressively during the study period. The increase in strength was correlated with more bone ingrowth and improved bone–tendon healing.

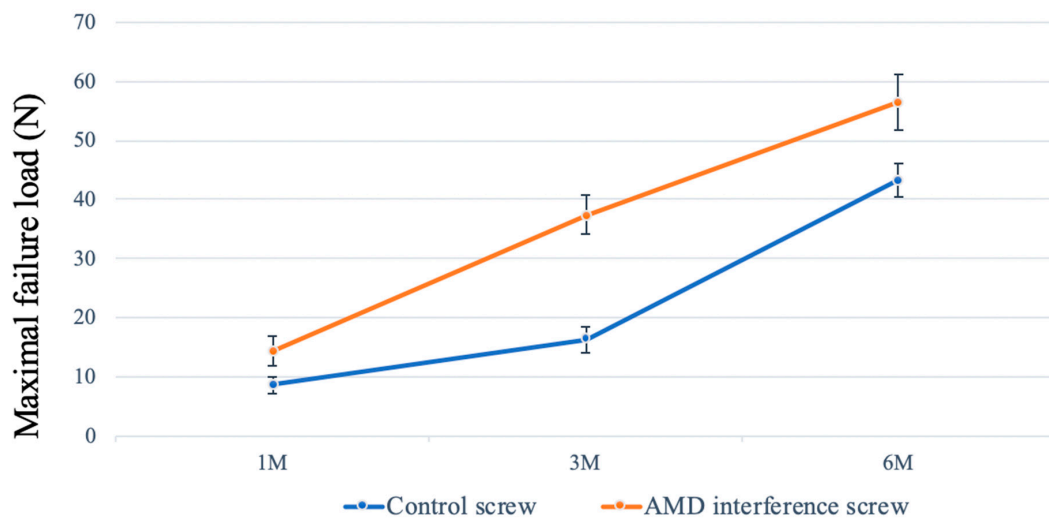


Figure 3. Biomechanical assessment. The mean maximal failure load in the AMD screw group was significantly higher than that in the control group at 1, 3, and 6 months ($p < 0.05$). The error bar denotes the standard deviation.

2.3. Micro-Computed Tomography Analysis

New bone formation between the implant and bone tissue was evaluated using micro-computed tomography (micro-CT), and the bone volume/tissue volume (BV/TV, %) and bone surface area/total volume (BS/TV, 1/mm) were quantified. The bone volume fraction and bone surface density were measured 100–1000 μm exterior to the implant, which represented the bone volume rate and bone surface rate for woven bone formation. Figure 4 illustrates dense new bone formation around the controlled and AMD screw in the tibial bone tunnel. The woven bone formed diffusely around the AMD screw with bone healed from the cancellous bone in the bone tunnel.

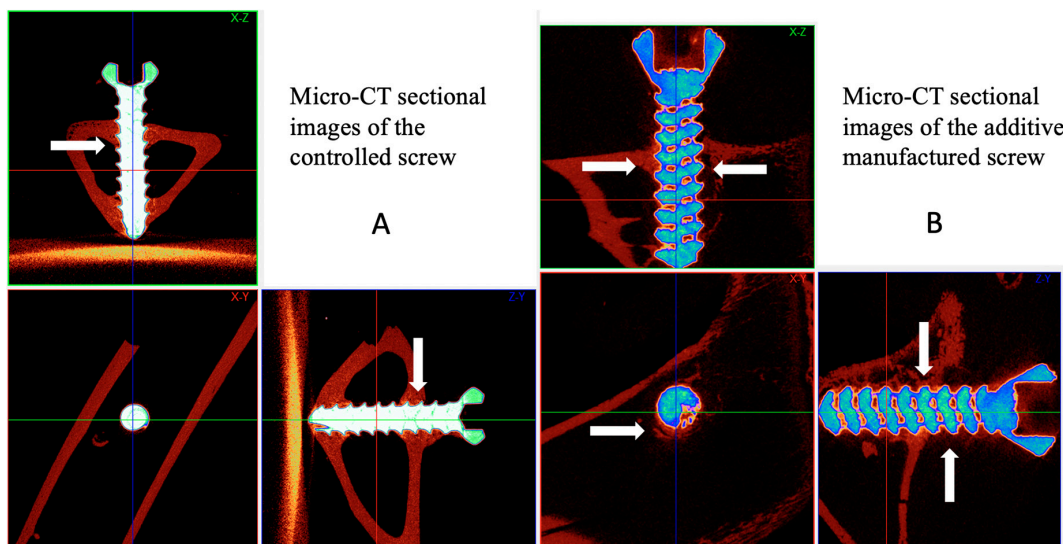


Figure 4. Micro-computed tomography (Micro-CT) examination. Comparison of micro-CT sectional images (A,B) between the interference screws. Micro-CT revealed woven bone formation between the AMD screw and bone tunnel in all sectional images. The AMD screw was fixed in the bone tunnel with massive bone ingrowth from the cancellous bone of the proximal tibia. Line arrows mark the woven bone formation.

In the quantitative evaluation of bone volume, we used a nonporous control screw as a template. Outer bone growth was defined as that exterior to the nonporous implant, and inner bone growth was defined as the bone inferior to the surface of the implant. The total bone volume was calculated using the accumulation of outer and inner bone growth. The total bone volume fraction (BV/TV) was significantly higher in the AMD group at the 1- and 3-month follow-ups (Figure 5; $p < 0.001$). The total bone surface density was significantly higher in 1-, 3-, and 6-month specimens for the AMD interference screw group. The ongrowth bone volume fraction was significantly higher in the AMD screw group at the 1-month follow-up. Because the control group did not have a porous structure, only the AMD screw group had bone ingrowth inferior to the surface of the implant. Subsequently, we evaluated the differences in the percent of ingrowth bone volume between different time points, and it was statistically significant between the 1- and 3-month follow-ups. No differences existed in outcomes for ingrowth bone surface density.

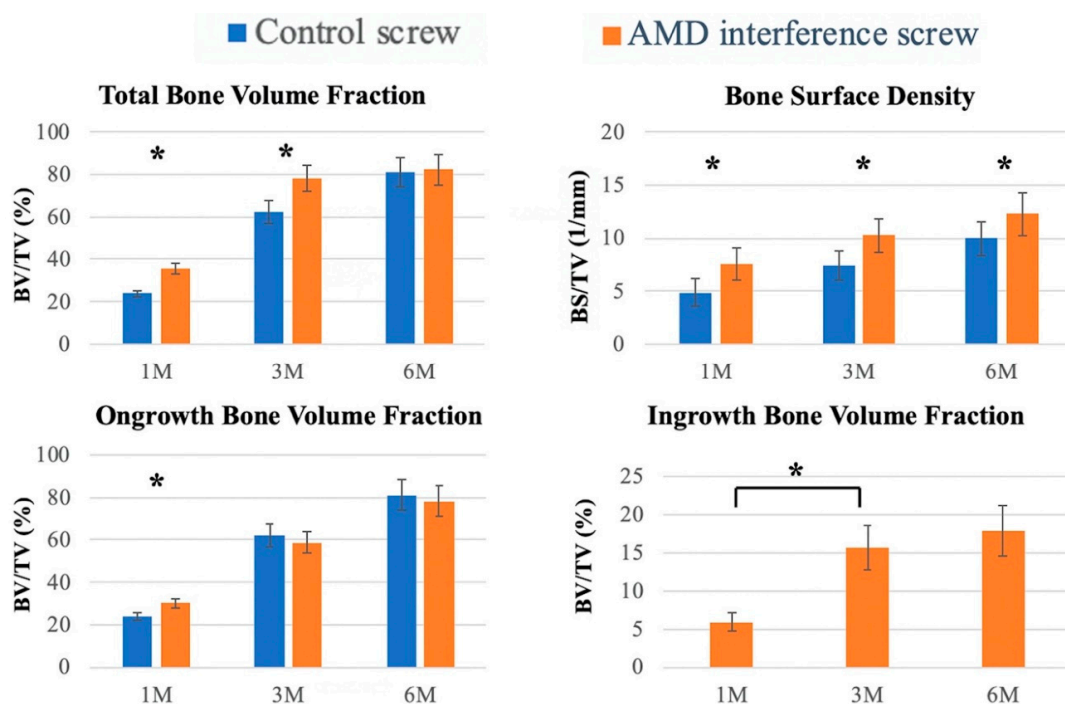


Figure 5. Quantitative evaluation of bone volume between bone and screw interfaces. Micro-CT was used to evaluate the bone ingrowth after screw implantation. Tissue volume (TV: mm^3), bone volume (BV: mm^3), and bone surface (BS: mm^2) were retrieved from 100 to 1000 μm above the implant. Bone volume fraction (BV/TV) and bone surface density (BS/TV) represent the bone volume rate and bone tissue surface rate, respectively. Ongoing bone volume denotes the bone outside the control screw, and ingrowth bone volume denotes bone mass inside the surface of the implant; the error bar represents the standard deviation, and * denotes statistical significance between the two groups.

2.4. Histology Analysis

In the histological examination, superior bone–screw integration was observed in the AMD screw group (Figure 6). The bioactive ceramic coating on the AMD screw makes the screw surface rough, which readily promotes bone ingrowth. In the control screw group, healing was identified at the bone–screw interface, where fibrous tissue covered the tip of the screw thread (Figure 6C,D). Moreover, bone ingrowth inside the AMD screw was identified as being because of the porous structure inside the screw (Figure 6G,H).

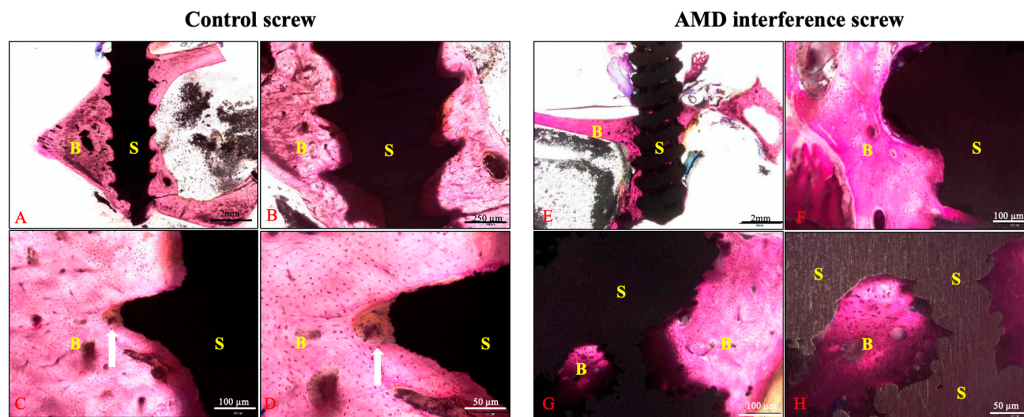


Figure 6. Histological examination of the bone–screw interface between groups. The specimens were stained with Sanderson’s Rapid Bone Stain and then counterstained with acid fuchsin. Figures (A–D) represented the controlled screw from scale of 12.5×, 40×, 100×, and 200×, respectively. The surface of the controlled screw was sharp and healed with fibrous tissue at the tip of screw thread. The AMD screw group (E–H) exhibited a rougher surface and superior bone–screw integration on the screw surface and inside the screw body. Line arrows indicate fibrous tissue healing at the tip of the control screw thread; B: bone, S: screw.

In the AMD screw group, the bone–screw interface was healed with more woven bone (Figure 7). The gap between the bone–screw construct was wider in the control group comparing with the AMD screw group. These findings were compatible with the micro-CT findings.

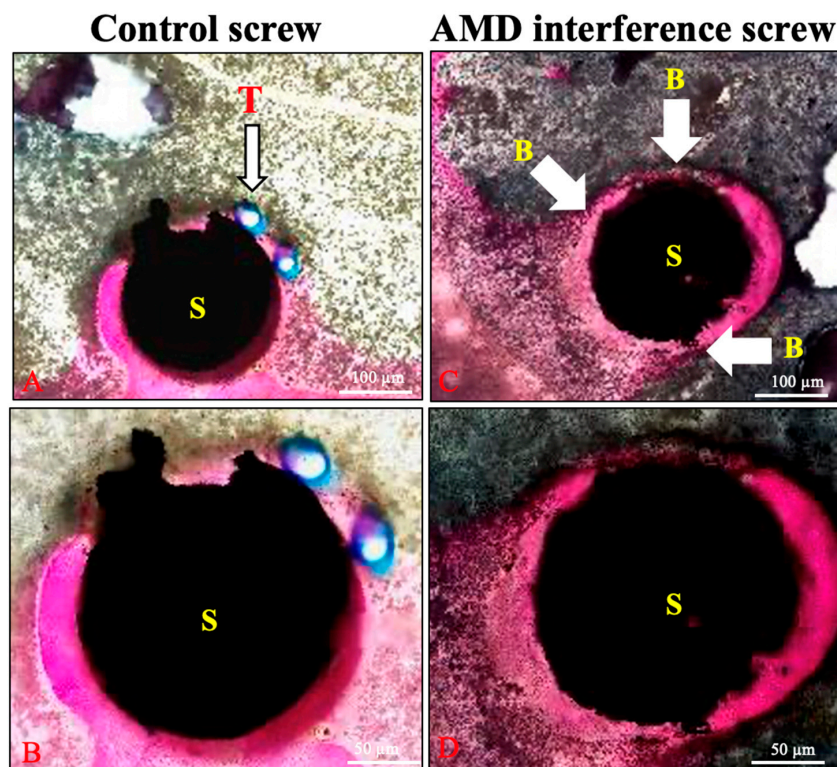


Figure 7. Histological examination of the 6-month specimens. More woven bone formation (wide arrows) was identified in the bone–screw construct in the AMD screw group. The tendon graft (line arrow) is shown between the screw and bone in the control group (A,B). The bone and screw were in close contact in the AMD screw group (C,D); B: bone, T: tendon, and S: screw.

3. Discussion

In this study, we designed an innovative AMD Ti screw with a ceramic surface modification for an animal study. For the biomechanical test, the AMD screw had a much stronger ultimate failure strength than the control, which indicated superior bone ingrowth in the bone–tendon–screw construct. A rough surface and porous structure have been reported to improve bone healing and reduce micromotion after screw implantation [19,27]. Such results are compatible with our study, where the total bone volume fraction was significantly higher at the 1- and 3-month follow-ups, which is crucial for graft healing after ACLR surgery. Because of fibrous tissue between the tendon–bone interface, a weak connection exists between tendon grafts and bones in ACLR, especially in the first 6 weeks [28]. Moreover, the bone surface density was significantly higher in our AMD screw group at all follow-ups, presenting more woven bone formation on the surface of the implants. These results not only reflect the porous structure on the AMD screw but also the surface modification that occurred with CaP apatite. In the SEM images, the feather-like apatite evident on the surface improved the bone tissue integration. This was also proved by the histological images, where the bone was observed to have healed to the screw more prominently instead of fibrous tissue forming. Our findings indicated that the AMD screw with ceramic bioactive surface modification could improve early woven bone formation and implant stability with a stronger ultimate pull-out load.

Surface modification has been demonstrated to be an effective strategy to accelerate bone healing at early implantation times. Coating with a layer of HA is one of the most commonly used methods because of its excellent biocompatible and osteoconductive properties [29]. Coating orthopedic Ti₆Al₄V with HA produces an osteoconductive surface that promotes early bone integration and minimizes the prosthesis loosening rate [30]. The capacity of HA to immobilize growth factors and proteins through noncovalent interactions improves the healing process [31,32]. However, delamination and fragmentation of HA has been reported [33], either caused by structural defects between the coating and implant or structural nonhomogeneity in terms of thickness and crystallinity [14]. The difference in the thermal expansion coefficient between HA and the implant induces interface stress and further poor adhesion [14]. Moreover, plasma spraying of HA does not produce a completely crystalline layer, which can cause the amorphous component to disappear from the HA coating, leading to its instability [34]. Wet chemical techniques can be used to form a thin film with strong bonding of the CaP coating and reduce the risk of film delamination and inflammatory reactions [35]. The surface-modified material is immersed in a CaP solution, such as SBF with pH and ion concentrations equal to human blood plasma [36]. Wet chemical techniques allow the immobilization of biofunctional substances within the CaP layer, such as bone morphogenetic protein [37], proteins [38], vitamins [39], and antibacterial agents [40]. Nguyen et al. demonstrated that sol–gel-formed CaP coatings improve bone ingrowth and increase bone-to-implant contact [35]. Nishiguchi et al. demonstrated that alkali- and heat-treated Ti result in strong bone bonding and a high ongrowth rate [41]. In another study, the osteoconduction of CaP coating was initiated with decreased local pH and partial dissolution of the coating for calcium and phosphate release [42]. The ions' reprecipitation and incorporation of proteins stimulated chemotaxis for bone conduction. In our study, we demonstrated enhanced and early bone ingrowth in the AMD screw with a bioactive ceramic surface modification, a finding that demonstrated a synergistic relationship between the CaP modified surface and bone tissue.

AM has great potential for personalized medicine in bone scaffolds and orthopedic implants [19]. AM techniques have been employed for orthopedic applications, such as the reconstruction of hips [23], knees [43], and clavicles [44]. The advantages of AM are that it creates porous and rough surfaces, which induce bone ingrowth [24]. Higher friction resistance may cause lower micromotions of the bone–implant construct for enhanced tissue integration [45]. Moreover, different pore sizes were shown to alter the progression of osteogenesis [46]. Significant differences in bone volume fraction and bone surface rate suggested superior bone ingrowth especially on the surface of the AMD screw. Bone growth clearly increased the stability of the implant and enhanced mechanical load failure. In our study, the AMD screw with surface modification was able to improve healing in the bone–tendon–screw

construct. AM offers new possibilities for improving long-term metal implant fixation. Richard et al. showed that using additive manufactured method could achieve maximal pull-out force with optimal design [47]. Bone is a 3D inhomogeneous structure which can be classified as compact bone (cortical bone) and trabecular bone (cancellous bone) with different porosity [48]. Moreover, the Young's modulus of human bone is much lower than the solid metals. AM technique can provide new design with maximal porous design and adequate resistance force, which is very difficult to accomplish through traditional method [19].

Although our results are encouraging, this study still had some limitations. First, the AMD interference screw had a similar morphology to the control screw. However, the nonporous structure and smooth surface of the commercial Ti screw were different from the AMD screw. Relevant studies have reported differences in pore size and surface roughness integration [49]. However, the ideal pore size of AMD screws has not been evaluated. The minimum pore size is considered to be approximately 100 μm because of cell size, migration, and transport. However, larger pore sizes are considered to enhance capillary formation and osteogenesis [46]. Second, this study used an extra-articular animal model, which differed from ACLR. The axis of the tibial tunnel was different, and the graft tunnel was not connected to the knee joint. Therefore, a positive effect in this model could not be confirmed for ACLR. Further animal studies using AMD screws with bioactive coating should be designed.

4. Materials and Methods

4.1. Study Design

In accordance with national animal welfare legislation and the National Institute of Health guidelines for the use of laboratory animals, this animal study was pre-approved by the Ethics Committee of the Industrial Technology Research Institute, Biomedical Technology and Device Research Laboratories, Taiwan (Approval No. MI-20190602, 03 June 2019). Twenty-seven New Zealand white rabbits (Master Laboratory Co., Ltd., Taipei City, Taiwan) with a mean body weight of 3.2 ± 0.4 kg and age of 6 months were selected. Using computer-generated randomization, a traditionally made Ti screw was implanted in one of the stifle joints (the control group) and an AMD porous screw with bioceramic coating was implanted in the other stifle joint of the same rabbit (the experimental group). All rabbits were divided into three groups based on implantation periods of 1, 3, and 6 months (nine in each group). In each group, three rabbits were used for the histological analysis, and the other six rabbits were used for micro-CT and biomechanical studies. For each animal, micro-CT analyses were performed immediately at the end of each experiment, and then the specimens were fresh-frozen for further biomechanical study.

4.2. Production of the Innovative Interference Screw

This study's controlled Ti screws were obtained from an AO cortical screw (DePuy Synthes, Johnson and Johnson, New Brunswick, NJ, USA) with a screw body length of 12 mm, core diameter of 1.8 mm, thread diameter of 2.1 mm, head diameter of 2.4 mm, and pitch of 1.0 mm, as shown in Figure 8.

The AMD Ti-6Al-4V screws were fabricated using selective laser melting, and a porous structure with a porosity of approximately 15.4% was formed during the AM process with the EOSINT M 280 system. The AMD screw was a template and evolved from the control screw with identical mechanical parameters of length, core diameter, thread diameter, head diameter, and pitch. Subsequently, the outer surface of the AMD screw was modified through a bioactive ceramic coating. Bioactive surface modification with porous Ti was performed using a chemical and heat treatment method. The main processing procedure was as follows. The sample was (1) ultrasonically cleaned; (2) soaked in 1 M NaOH solution at 60 °C for 24 h; (3) soaked in 100 mM CaCl₂ solution at 40 °C for 24 h; (4) cleaned with distilled water and dried; (5) heated to 600–800 °C for 1 h at a heating rate of 5 °C/min; (6) after

cooling, it was soaked in alkaline pH 7.4 SBF containing NaCl, NaHCO₃, KCl, K₂HPO₄, MgCl₂, CaCl₂, and Na₂SO₄ for 3 days.

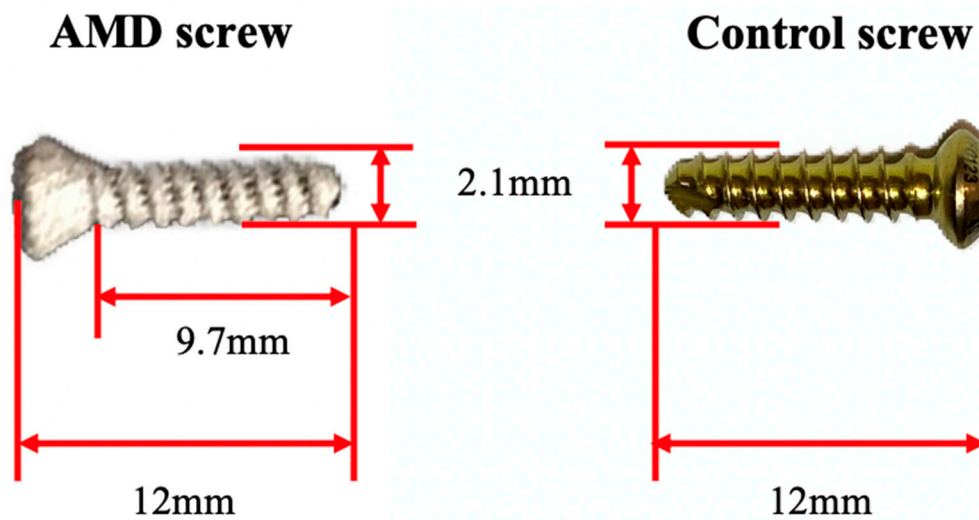


Figure 8. Illustration of a porous AMD screw. The control interference screw was made with Ti and had a screw body length of 12 mm, core diameter of 1.8 mm, thread diameter of 2.1 mm, head diameter of 2.4 mm, and pitch of 1.0 mm (Depuy Synthes, Johnson and Johnson, New Brunswick, NJ, USA). The AMD screw with a similar morphology was produced using an EOSINT M 280 laser sintering system (EOS GmbH, Munich, Germany). The AMD interference screws received NaOH and heat treatments for bioactive ceramic surface modification.

After chemical surface modification, the AMD screws formed a dense and uniform bone-like apatite layer (approx. thickness = 1 μ m) on the metal surface in SBF solution. This apatite coating was expected to enable the use of bioactive Ti-6Al-4V implants as artificial bones to enhance bone growth. Figure 7 presents a comparison of the control and AMD screws with bioactive ceramic coating.

4.3. Surgical Procedures

All rabbits received a preoperative dose of intramuscular cefazolin sodium (0.1 mg/kg) as a prophylactic antibiotic. A Zoletil–Rompun mixture (Zoletil 15 mg/kg [Virbac Taiwan, Taiwan] + Rompun 0.05 mL/kg [Bayer Taiwan, Taiwan]) was intramuscularly injected to induce general anesthesia. For analgesia, the rabbits were administered meloxicam (0.15 mg/kg peroral; Metacam, Boehringer Ingelheim Taiwan, Taiwan) 1 day preoperatively, immediately preoperatively, and 2 days following surgery.

We used an animal model similar to that developed by Yamakado et al. [50] with some modifications. First, we made a lateral parapatellar approach on the bilateral knee to approach the lateral femoral condyle. The tendon of the extensor digitorum longus (EDL) was detached from its origin. A drill hole (diameter: 2.0 mm) was created using an electrical drill at the proximal tibial metaphysis perpendicular to the long axis of the tibia. The EDL tendon was passed through the bone tunnel and transfixed with the interference screw from the medial to lateral side while the paw was supported in dorsiflexion. We repaired the joint capsule, muscles, and fascia with 4-0 Vicryl sutures. After surgery, the rabbits were allowed to freely exercise in the same cage without restrictions. All animals were ambulant without any protection or immobilization. Euthanasia was performed through injecting an intravenous overdose of pentobarbital. Stifle joints were stored at -20°C for further analyses.

4.4. Microscopic Observation

Microscopic observation was carried out using a scanning electron microscope (SEM; TM 1000, Hitachi) and the morphology of bioactive ceramic coating was observed. SEM observation was

with an operating voltage of 15 kV and the vacuum level of the observation chamber was 10^{-5} to Pa. Transmission electron micrograph (TEM) and energy dispersive X-ray analysis (EDX) was used to evaluate the chemical component of bioactive apatite. TEM images were obtained using a JEOL transmission electron micrograph (JEM-2100F, JEOL, MA, USA) at 200 kV. Energy Dispersive X-ray analysis was used to identify the chemical element of bioactive apatite. EDX measurement were performed on a JSX-1000S Fluorescence Spectrometer X-ray analyzer (JEOL, MA, USA). The EDX spectrum was obtained at an acceleration of 20 kV and collected for 19 seconds.

4.5. Biomechanical Analysis

Six rabbits from each group were selected for a biomechanical test. We carefully dissected the EDL tendon from the distal end of insertion and removed all other redundant tissue. We used a material testing machine (ElectroForce 3510-AT; Bose Corporation, Framingham, MA, United States) for biomechanical testing. The graft was secured on the clamps at a distance of 3 cm from the lateral tibial aperture, allowing tensile loading along the long axis of the tibial bone tunnel at a strain rate of 0.5 mm/min until failure occurred. The ultimate pull-out load and failure mode were recorded and analyzed.

4.6. Micro-Computed Tomography Analysis

Six rabbits from each group were sacrificed at 1, 3, and 6 months postoperatively. Micro-CT was used to evaluate the new bone formation in the bone–screw interface. The specimens were prepared for micro-CT evaluation (Skyscan 1176 μ CT System; Bruker, Kontich, Belgium). High-voltage scanning (voltage: 90 kVp, current: 278 μ A, at a 25 W output with a 360° scan) and an 18- μ m sample size were used for this experiment. Cross-sectional images were reconstructed, and the region of interest was further selected. We performed the analyses with 1.5 mm specimen for 100 slice images. The tissue volume (TV, mm^3), bone volume (BV, mm^3), bone volume fraction (BV/TV, %), bone surface (BS, mm^2), and bone surface rate (BS/TV, 1/mm) were retrieved from 100 to 1000 μ m above the metal implant. We used a nonporous implant as a template; outer bone growth was defined as that exterior to the nonporous implant surface, and inner bone growth was defined as the bone formation interior to the surface of the implant. The total bone growth indicated the sum of the outer and inner bone growth.

4.7. Histological Analysis

The last three rabbits were sacrificed for histological examination. The specimens were fixed with 10% formalin for several days and decalcified with graded series of alcohol. The proximal tibia was embedded in paraffin and sliced into approximately 150- μ m slices using an IsoMet Low Speed Saw (Buehler, Lake Bluff, IL, United states) and ground to 60 μ m with a grinding/polishing machine. The samples were sectioned perpendicular to the long axis of the tibia tunnel. Staining was performed using Sanderson's Rapid Bone Stain (Dorn and Hart Microedge, Loxley, AL, USA) and then counterstained with acid fuchsin. Histological sections were examined using a light microscope (Nikon ECLIPSE, Melville, NY, USA).

4.8. Statistical Analysis

Before the animal study, a power analysis was performed to calculate the number of animals needed to prevent type II errors. In our previous study, micro-CT revealed the bone volume fraction (BV/TV) to be 39.0 ± 6.7 % for the experimental tibia [26]. Six specimens per group achieved a power of 0.80 with $\alpha = 0.05$. All data were expressed as mean \pm standard deviation. The obtained biomechanical test and CT data were compared using paired *t* tests. All statistical analyses were performed using the SPSS 18.0 software package (SPSS, Chicago, IL, USA). The results were considered statistically significant at $p < 0.05$.

5. Conclusions

In this study, a bioactive ceramic coating was produced on Ti metal using chemical and heat treatments. The AMD screw achieved a higher ultimate pull-out strength and a larger amount of woven bone formation than the control; furthermore, the innovative screw implantation in the rabbit model resulted in enhanced bone integration and stability in the bone–tendon–screw construct.

Author Contributions: Investigation and writing: Y.-M.H., C.-C.H., P.-IT., K.-Y.Y.; Project administration: S.-IH., H.-H.S., S.-W.H., C.-Y.C.; Results evaluation/Supervision: H.-J.L., S.-Y.C., F.-H.L., C.-Y.C. All authors have read and agreed to the published version of the manuscript.

Funding: This research was funded by Industrial Technology Research Institute: J356EX3200.

Acknowledgments: This article was subsidized by Ministry of Science and Technology and National Taiwan University (NTU), Taiwan.

Conflicts of Interest: The authors declare no conflict of interest.

References

1. Chalmers, P.N.; Mall, N.A.; Moric, M.; Sherman, S.L.; Paletta, G.P.; Cole, B.J.; Bach, B.R. Does ACL reconstruction alter natural history?: A systematic literature review of long-term outcomes. *J. Bone Jt. Surg.* **2014**, *96*, 292–300. [[CrossRef](#)] [[PubMed](#)]
2. Brand, J.; Weiler, A.; Caborn, D.N.; Brown, C.H.; Johnson, D.L. Graft fixation in cruciate ligament reconstruction. *Am. J. Sports Med.* **2000**, *28*, 761–774. [[CrossRef](#)] [[PubMed](#)]
3. De Wall, M.; Scholes, C.J.; Patel, S.; Coolican, M.R.J.; Parker, D.A. Tibial fixation in anterior cruciate ligament reconstruction: A prospective randomized study comparing metal interference screw and staples with a centrally placed polyethylene screw and sheath. *Am. J. Sports Med.* **2011**, *39*, 1858–1864. [[CrossRef](#)] [[PubMed](#)]
4. Arama, Y.; Salmon, L.J.; Sri-Ram, K.; Linklater, J.; Roe, J.P.; Pinczewski, L.A. Bioabsorbable Versus Titanium Screws in Anterior Cruciate Ligament Reconstruction Using Hamstring Autograft: A Prospective, Blinded, Randomized Controlled Trial With 5-Year Follow-up. *Am. J. Sports Med.* **2015**, *43*, 1893–1901. [[CrossRef](#)]
5. Laupattarakasem, P.; Laopaiboon, M.; Kosuwon, W.; Laupattarakasem, W. Meta-analysis comparing bioabsorbable versus metal interference screw for adverse and clinical outcomes in anterior cruciate ligament reconstruction. *Knee Surg. Sports Traumatol. Arthrosc.* **2014**, *22*, 142–153. [[CrossRef](#)]
6. Kramer, D.E.; Kalish, L.A.; Kocher, M.S.; Yen, Y.-M.; Micheli, L.J.; Heyworth, B.E. Complications of Bioabsorbable Tibial Interference Screws after Anterior Cruciate Ligament Reconstruction in Pediatric and Adolescent Athletes. *Orthop. J. Sports Med.* **2020**, *8*, 2325967120904010. [[CrossRef](#)]
7. Mercado, C.; Seeley, Z.; Bandyopadhyay, A.; Bose, S.; McHale, J.L. Photoluminescence of dense nanocrystalline titanium dioxide thin films: Effect of doping and thickness and relation to gas sensing. *ACS Appl. Mater. Interfaces* **2011**, *3*, 2281–2288. [[CrossRef](#)]
8. White, R.A.; Weber, J.N.; White, E.W. Replamineform: A new process for preparing porous ceramic, metal, and polymer prosthetic materials. *Science* **1972**, *176*, 922–924. [[CrossRef](#)]
9. Clemow, A.J.; Weinstein, A.M.; Klawitter, J.J.; Koeneman, J.; Anderson, J. Interface mechanics of porous titanium implants. *J. Biomed. Mater. Res.* **1981**, *15*, 73–82. [[CrossRef](#)]
10. Xue, W.; Krishna, B.V.; Bandyopadhyay, A.; Bose, S. Processing and biocompatibility evaluation of laser processed porous titanium. *Acta Biomater.* **2007**, *3*, 1007–1018. [[CrossRef](#)]
11. LeGeros, R.Z. Properties of osteoconductive biomaterials: Calcium phosphates. *Clin. Orthop. Relat. Res.* **2002**, *395*, 81–98. [[CrossRef](#)]
12. Ducheyne, P.; Qiu, Q. Bioactive ceramics: The effect of surface reactivity on bone formation and bone cell function. *Biomaterials* **1999**, *20*, 2287–2303. [[CrossRef](#)]
13. Gross, K.A.; Berndt, C.C. Thermal processing of hydroxyapatite for coating production. *J. Biomed. Mater. Res.* **1998**, *39*, 580–587. [[CrossRef](#)]
14. Yang, Y.C.; Chang, E. Influence of residual stress on bonding strength and fracture of plasma-sprayed hydroxyapatite coatings on Ti-6Al-4V substrate. *Biomaterials* **2001**, *22*, 1827–1836. [[CrossRef](#)]
15. Yang, C.Y.; Wang, B.C.; Lee, T.M.; Chang, E.; Chang, G.L. Intramedullary implant of plasma-sprayed hydroxyapatite coating: An interface study. *J. Biomed. Mater. Res.* **1997**, *36*, 39–48. [[CrossRef](#)]

16. Du, C.; Meijer, G.J.; van de Valk, C.; Haan, R.E.; Bezemer, J.M.; Hesselting, S.C.; Cui, F.Z.; de Groot, K.; Layrolle, P. Bone growth in biomimetic apatite coated porous Polyactive 1000PEGT70PBT30 implants. *Biomaterials* **2002**, *23*, 4649–4656. [[CrossRef](#)]
17. Aniket; Young, A.; Marriott, I.; El-Ghannam, A. Promotion of pro-osteogenic responses by a bioactive ceramic coating. *J. Biomed. Mater. Res. A* **2012**, *100*, 3314–3325.
18. Kokubo, T.; Yamaguchi, S. Novel Bioactive Titanate Layers Formed on Ti Metal and Its Alloys by Chemical Treatments. *Materials* **2010**, *3*, 48–63. [[CrossRef](#)]
19. Wang, X.; Xu, S.; Zhou, S.; Xu, W.; Leary, M.; Choong, P.; Qian, M.; Brandt, M.; Xie, Y.M. Topological design and additive manufacturing of porous metals for bone scaffolds and orthopaedic implants: A review. *Biomaterials* **2016**, *83*, 127–141. [[CrossRef](#)]
20. Tappa, K.; Jammalamadaka, U.; Weisman, J.A.; Ballard, D.H.; Wolford, D.D.; Pascual-Garrido, C.; Wolford, L.M.; Woodard, P.K.; Mills, D.K. 3D Printing Custom Bioactive and Absorbable Surgical Screws, Pins, and Bone Plates for Localized Drug Delivery. *J. Funct. Biomater.* **2019**, *10*, 17. [[CrossRef](#)]
21. Kaye, R.; Goldstein, T.; Zeltsman, D.; Grande, D.A.; Smith, L.P. Three dimensional printing: A review on the utility within medicine and otolaryngology. *Int. J. Pediatr. Otorhinolaryngol.* **2016**, *89*, 145–148. [[CrossRef](#)] [[PubMed](#)]
22. Perticarini, L.; Zanon, G.; Rossi, S.M.P.; Benazzo, F.M. Clinical and radiographic outcomes of a trabecular titanium™ acetabular component in hip arthroplasty: Results at minimum 5 years follow-up. *BMC Musculoskelet. Disord.* **2015**, *16*, 375–376. [[CrossRef](#)] [[PubMed](#)]
23. Arabnejad, S.; Johnston, B.; Tanzer, M.; Pasini, D. Fully porous 3D printed titanium femoral stem to reduce stress-shielding following total hip arthroplasty. *J. Orthop. Res.* **2017**, *35*, 1774–1783. [[CrossRef](#)] [[PubMed](#)]
24. Mullen, L.; Stamp, R.C.; Fox, P.; Jones, E.; Ngo, C.; Sutcliffe, C.J. Selective laser melting: A unit cell approach for the manufacture of porous, titanium, bone in-growth constructs, suitable for orthopedic applications. II. Randomized structures. *J. Biomed. Mater. Res. Part B Appl. Biomater.* **2010**, *92*, 178–188. [[CrossRef](#)] [[PubMed](#)]
25. Wauthle, R.; Ahmadi, S.M.; Amin Yavari, S.; Mulier, M.; Zadpoor, A.A.; Weinans, H.; Van Humbeeck, J.; Kruth, J.-P.; Schrooten, J. Revival of pure titanium for dynamically loaded porous implants using additive manufacturing. *Mater. Sci. Eng. C Mater. Biol. Appl.* **2015**, *54*, 94–100. [[CrossRef](#)]
26. Tsai, P.-I.; Chen, C.-Y.; Huang, S.-W.; Yang, K.-Y.; Lin, T.-H.; Chen, S.-Y.; Sun, J.-S. Improvement of bone-tendon fixation by porous titanium interference screw: A rabbit animal model. *J. Orthop. Res.* **2018**, *36*, 2633–2640. [[CrossRef](#)]
27. Sing, S.L.; An, J.; Yeong, W.Y.; Wiria, F.E. Laser and electron-beam powder-bed additive manufacturing of metallic implants: A review on processes, materials and designs. *J. Orthop. Res.* **2016**, *34*, 369–385. [[CrossRef](#)]
28. Tomita, F.; Yasuda, K.; Mikami, S.; Sakai, T.; Yamazaki, S.; Tohyama, H. Comparisons of intraosseous graft healing between the doubled flexor tendon graft and the bone-patellar tendon-bone graft in anterior cruciate ligament reconstruction. *Arthroscopy* **2001**, *17*, 461–476. [[CrossRef](#)]
29. Arcos, D.; Vallet-Regí, M. Substituted hydroxyapatite coatings of bone implants. *J. Mater. Chem. B* **2020**, *8*, 1781–1800. [[CrossRef](#)]
30. Tanzer, M.; Kantor, S.; Rosenthal, L.; Bobyn, J.D. Femoral remodeling after porous-coated total hip arthroplasty with and without hydroxyapatite-tricalcium phosphate coating: A prospective randomized trial. *J. Arthroplasty* **2001**, *16*, 552–558. [[CrossRef](#)]
31. Zambonin, G.; Camerino, C.; Greco, G.; Patella, V.; Moretti, B.; Grano, M. Hydroxyapatite coated with heaptocyte growth factor (HGF) stimulates human osteoblasts in vitro. *J. Bone Jt. Surg. Br.* **2000**, *82*, 457–460. [[CrossRef](#)] [[PubMed](#)]
32. Matsumoto, T.; Okazaki, M.; Inoue, M.; Yamaguchi, S.; Kusunose, T.; Toyonaga, T.; Hamada, Y.; Takahashi, J. Hydroxyapatite particles as a controlled release carrier of protein. *Biomaterials* **2004**, *25*, 3807–3812. [[CrossRef](#)] [[PubMed](#)]
33. Ducheyne, P.; Cuckler, J.M. Bioactive ceramic prosthetic coatings. *Clin. Orthop. Relat. Res.* **1992**, 102–114. [[CrossRef](#)]
34. Zyman, Z.; Weng, J.; Liu, X.; Zhang, X.; Ma, Z. Amorphous phase and morphologica structure of hydroxyapatite plasma coatings. *Biomaterials* **1993**, *14*, 225–228. [[CrossRef](#)]
35. Nguyen, H.Q.; Deporter, D.A.; Pilliar, R.M.; Valiquette, N.; Yakubovich, R. The effect of sol-gel-formed calcium phosphate coatings on bone ingrowth and osteoconductivity of porous-surfaced Ti alloy implants. *Biomaterials* **2004**, *25*, 865–876. [[CrossRef](#)]

36. Aparecida, A.H.; Fook, M.V.L.; Guastaldi, A.C. Biomimetic apatite formation on Ultra-High Molecular Weight Polyethylene (UHMWPE) using modified biomimetic solution. *J. Mater. Sci. Mater. Med.* **2009**, *20*, 1215–1222. [[CrossRef](#)]
37. Yu, X.; Wang, L.; Jiang, X.; Rowe, D.; Wei, M. Biomimetic CaP coating incorporated with parathyroid hormone improves the osseointegration of titanium implant. *J. Mater. Sci. Mater. Med.* **2012**, *23*, 2177–2186. [[CrossRef](#)]
38. Hägi, T.T.; Enggist, L.; Michel, D.; Ferguson, S.J.; Liu, Y.; Hunziker, E.B. Mechanical insertion properties of calcium-phosphate implant coatings. *Clin. Oral Implants Res.* **2010**, *21*, 1214–1222. [[CrossRef](#)]
39. Ciobanu, G.; Ciobanu, O. Investigation on the effect of collagen and vitamins on biomimetic hydroxyapatite coating formation on titanium surfaces. *Mater. Sci. Eng. C Mater. Biol. Appl.* **2013**, *33*, 1683–1688. [[CrossRef](#)]
40. Zhao, L.; Chu, P.K.; Zhang, Y.; Wu, Z. Antibacterial coatings on titanium implants. *J. Biomed. Mater. Res. Part B Appl. Biomater.* **2009**, *91*, 470–480. [[CrossRef](#)]
41. Nishiguchi, S.; Fujibayashi, S.; Kim, H.-M.; Kokubo, T.; Nakamura, T. Biology of alkali- and heat-treated titanium implants. *J. Biomed. Mater. Res. A* **2003**, *67*, 26–35. [[CrossRef](#)] [[PubMed](#)]
42. Rahbek, O.; Overgaard, S.; Jensen, T.B.; Bendix, K.; Søballe, K. Sealing effect of hydroxyapatite coating: A 12-month study in canines. *Acta Orthop. Scand.* **2000**, *71*, 563–573. [[CrossRef](#)] [[PubMed](#)]
43. Liska, W.D.; Marcellin-Little, D.J.; Eskelinen, E.V.; Sidebotham, C.G.; Harrysson, O.L.A.; Hielm-Björkman, A.K. Custom total knee replacement in a dog with femoral condylar bone loss. *Vet. Surg.* **2007**, *36*, 293–301. [[CrossRef](#)] [[PubMed](#)]
44. Cronskär, M.; Rasmussen, J.; Tinnsten, M. Combined finite element and multibody musculoskeletal investigation of a fractured clavicle with reconstruction plate. *Comput. Methods Biomech. Biomed. Eng.* **2015**, *18*, 740–748. [[CrossRef](#)]
45. Harrison, N.; McHugh, P.E.; Curtin, W.; Mc Donnell, P. Micromotion and friction evaluation of a novel surface architecture for improved primary fixation of cementless orthopaedic implants. *J. Mech. Behav. Biomed. Mater.* **2013**, *21*, 37–46. [[CrossRef](#)]
46. Karageorgiou, V.; Kaplan, D. Porosity of 3D biomaterial scaffolds and osteogenesis. *Biomaterials* **2005**, *26*, 5474–5491. [[CrossRef](#)]
47. van Arkel, R.J.; Ghouse, S.; Milner, P.E.; Jeffers, J.R.T. Additive manufactured push-fit implant fixation with screw-strength pull out. *J. Orthop. Res.* **2018**, *36*, 1508–1518. [[CrossRef](#)]
48. Choi, K.; Kuhn, J.L.; Ciarelli, M.J.; Goldstein, S.A. The elastic moduli of human subchondral, trabecular, and cortical bone tissue and the size-dependency of cortical bone modulus. *J. Biomech.* **1990**, *23*, 1103–1113. [[CrossRef](#)]
49. Bansiddhi, A.; Sargeant, T.D.; Stupp, S.I.; Dunand, D.C. Porous NiTi for bone implants: A review. *Acta Biomater.* **2008**, *4*, 773–782. [[CrossRef](#)]
50. Yamakado, K.; Kitaoka, K.; Yamada, H.; Hashiba, K.; Nakamura, R.; Tomita, K. The influence of mechanical stress on graft healing in a bone tunnel. *Arthroscopy* **2002**, *18*, 82–90. [[CrossRef](#)]

